Journal of Colloid and Interface Science 505 (2017) 38–48

Contents lists available at ScienceDirect

Journal of Colloid and Interface Science

journal homepage: www.elsevier.com/locate/jcis

Regular Article

Versatile polyvinylidene fluoride hybrid ultrafiltration membranes with superior antifouling, antibacterial and self-cleaning properties for water treatment

Yuan-Wei Huang [a], Zuo-Ming Wang [b], Xi Yan [a,*], Jun Chen [b], Ya-Jun Guo [a], Wan-Zhong Lang [a,*]

[a] The Education Ministry Key Laboratory of Resource Chemistry and Shanghai Key Laboratory of Rare Earth Functional Materials, Department of Chemistry and Chemical Engineering, Shanghai Normal University, 100 Guilin Road, Shanghai 200234, China
[b] College of Life and Environment Sciences, Shanghai Normal University, 100 Guilin Road, Shanghai 200234, China

GRAPHICAL ABSTRACT

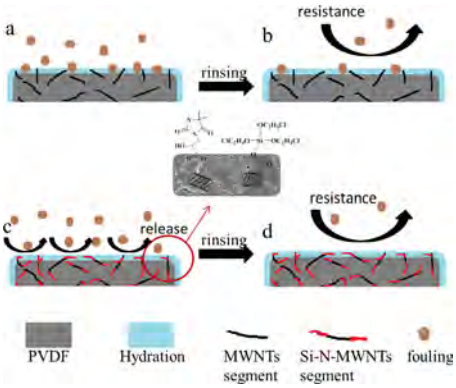

ARTICLE INFO

Article history:
Received 27 March 2017
Revised 23 May 2017
Accepted 23 May 2017
Available online 24 May 2017

Keywords:
N-halamine
Siloxane
multi-walled carbon nanotubes (MWNTs)
Antibacterial
Self-cleaning

ABSTRACT

Novel ultrafiltration membranes with both superior antibacterial and self-cleaning properties were fabricated. By using a non-solvent induced phase separation method (NIPS), N-halamine epoxide and siloxane were grafted onto the multi-walled carbon nanotubes (N-Si-MWNTs) to fabricate polyvinylidene fluoride (PVDF) hybrid membranes. The membrane morphology was observed under a field emission scanning electron microscopy. The results demonstrated that the PVDF hybrid membranes had an asymmetrical structure, and their hydraulic permeability was evidently enhanced with the addition of modified MWNTs. When compared with the primitive PVDF membrane, the hybrid membranes presented improved surface hydrophilicity. After three ultrafiltration–regeneration cycles with bovine serum albumin as model biofoulant and pure water as detergent, the PVDF hybrid membranes exhibited a high flux recovery ratio (FRR). Furthermore, when compared with other membranes, the membrane containing N-Si-MWNTs displayed the highest FRR value of above 96.5% after the entire fouling and cleaning experiment. The fabricated PVDF/N-Si-MWNTs hybrid membranes had excellent antibacterial efficacy, presenting maximum antibacterial efficacy of 98.0% and 95.6% against *Staphylococcus aureus* and *Escherichia coli*, respectively. Thus, the PVDF/N-Si-MWNTs membranes fabricated in this study are environment-friendly with both benign antibacterial and self-cleaning properties.

* Corresponding authors.
E-mail addresses: yanxi@shnu.edu.cn (X. Yan), wzlang@shnu.edu.cn (W.-Z. Lang).

http://dx.doi.org/10.1016/j.jcis.2017.05.076
0021-9797/

Nomenclature

ω_1	wet weights of the membrane	ΔP	trans-membrane pressure (bar)
ω_2	dry weights of the membrane	μ	filtrate viscosity (Pa S)
l	the membrane thickness (m)	R_t	total permeation resistance of membrane (m^{-1})
d_w	the water density (0.998 g/cm^3)	R_m	intrinsic membrane resistance (m^{-1})
R	the solute rejection rate (%)	R_r	irreversible resistance (m^{-1})
C_p	the concentrations of permeate (g/L)	R_{ir}	reversible resistance (m^{-1})
C_F	the concentrations of feed solutions (g/L)	N	the normality of the consumed NaS_2O_3 in the titration (equiv. L^{-1})
Q	volumetric flow rate (m^3)	V	the volume of the consumed NaS_2O_3 in the titration (L)
a	valid membrane area (m^2)	W	the weight of membrane sample (g)
J_{BSA}	BSA aqueous solution permeation flux (m/s)	E	sterilization ratio (%)
J_R	water flux of cleaned membrane after each cycle (m/s)	A	the number of visible bacterial colonies contacting with membrane
J_w	initial pure water flux (m/s)	B	the number of visible bacterial colonies without contacting membrane
FRR	pure water flux recovery ratio		
PWP	pure water permeation (L $m^{-2}bar^{-1}$ h^{-1})		
J	membrane permeation flux in filtration process (m/s)		

1. Introduction

Ultrafiltration technology has been widely used as an effective approach for applications in drinking water treatment and waste water drainage and reuse treatment. However, membrane fouling, including biofouling and organic fouling, decreases the ultrafiltration efficiency and shortens membrane life. Therefore, membrane surfaces with both superior antibacterial and self-cleaning properties are the most attractive owing to their long-standing diverse functions. Moreover, fabrication of novel membranes based on these features would promote surface-governed or surface-based technologies for industrial, medical, environmental, and marine applications. The key to achieve superior antibacterial and self-cleaning properties is to design rational material and prepare homologous membranes [1,2]. Currently, antibacterial and self-cleaning properties are often achieved separately. While modified multi-walled carbon nanotubes (MWNTs), metal nanoparticles, and, particularly, amphiphilic nanofillers have been widely used to fabricate antibacterial membranes [3–5], hydrophilic antifouling surfaces and hydrophobic self-cleaning surfaces have been utilized to develop low-fouling and non-fouling surfaces [6].

Various approaches have been employed to fabricate antifouling and self-cleaning membranes. For example, zwitterionic monomer ([3-(methacryloylamino)propyl]-dimethyl(3-sulfopropyl) ammonium hydroxide inner salt) and side-chain fluorinated methacrylate monomer with sodium dodecyl sulfate (SDS) as emulsifier were used to prepare amphiphilic copolymers via aqueous phase emulsion polymerization, and the product was used as an additive to fabricate antifouling and self-cleaning membranes. The permeation flux recovery of the resultant membranes reached nearly 100% [6]. In another study, hydrophilic poly (ethylene oxide) (PEO) and polydimethylsiloxane (PDMS) segments were constructed via free-radical polymerization. The resultant fabricated membranes presented antifouling and self-cleaning properties, and also exhibited a visible decline in irreversible and reversible flux and complete retention of permeation flux recovery [7].

Nowadays, polyvinylidene fluoride (PVDF) is widely used for the development of ultrafiltration membrane owing to its good chemical resistance, thermal and hydrolytic stability, and mechanical strength. However, its hydrophobicity often leads to organic fouling and biofouling. Several nanofillers such as aluminum oxide, titanium dioxide nanoparticles, zinc oxide, silicon oxide, and silver nanoparticles have been utilized to modify PVDF membranes [8–16], and have presented positive effects on membrane properties. In recent years, MWNTs have been considerably used in modifying membranes because of their outstanding properties such as high specific area, prominent mechanical properties, and workability [17–20]. Nevertheless, crude MWNTs are difficult to disperse in casting solution owing to electrostatic influence, and opportune chemical modifications have been used to overcome this limitation. Strong acid has been commonly utilized to oxidize MWNTs and increase their dispersion and workability [21–24].

Currently, metal ions, quaternary ammonium salts, and N-halamines are widely employed to fabricate antimicrobial membranes. Among them, N-halamines are outstanding antibacterial agents owing to their excellent stability, biocidal efficacy, low toxicity, low corrosion of surfaces, and relatively economical properties [25–28]. Several tethering, grafting, and polymerization methods have been employed to anchor the antibacterial N-halamine moieties to membrane surfaces [4]. In general, chemical cleaning is commonly used to regenerate fouled membranes. Although chemical cleaning usually achieves a relatively high pure water flux recovery ratio (FRR), it destroys membrane properties and structure. Membrane cleaning with pure water alone may not achieve the desired FRR, and low surface energy architecture is generally employed in self-cleaning surfaces. For instance, hydrophobic polymers such as silicone-based and fluorinated polymers have been widely used through coating or grafting [29–31]. The mechanism of self-cleaning is to prevent the deposition and adsorption of foulants. As low surface energy architecture could decrease the interaction between membrane surfaces and foulants, the foulants could be rinsed using low water pressure, which has been generally recorded as fouling release [2,32,33]. Some of the recent representative studies on antifouling, self-cleaning, or antibacterial membranes are summarized in Table 1.

In the present study, novel PVDF ultrafiltration membranes simultaneously possessing antifouling, antibacterial, and self-cleaning properties were fabricated. In brief, MWNTs were oxidized by nitric acid steam (O-MWNTs), grafted with N-halamine and siloxane (N-Si-MWNTs), and used as nanofillers to fabricate PVDF hybrid membranes by non-solvent induced phase separation method (NIPS). Addition of N-halamine (derived from 5, 5-dimethylhydantoin) and siloxane ensured both antibacterial and self-cleaning properties. The effects of N-Si-MWNTs addition on the morphology, permeation, antibacterial performance, and self-cleaning efficiency of the final fabricated membranes were studied. To confirm the self-cleaning property of the resultant membranes, deionized water was used to rinse the fouled membranes. The bacteriostatic rates of the fabricated membranes were evaluated

Table 1
The recent studies related to anti-fouling or self-cleaning or antibacterial membranes.

Refs.	Year	Modulus	Pure water flux (L M^{-2} h^{-1} bar^{-1})	FRR (%)	Rejection ratios (%)	Antibacterial rate (%)
Liu [34]	2013	PVDF graft amphiphilic copolymer	126.6	89.2	93.8[a]	/
Duan [35]	2015	PES/Cu NPs @HNTs	212	/	>80[b]	94.5 (*E.coli*)[d]
Li [36]	2014	PES-g- HPG	/	>94	/	93.7 (*E.coli*)
Li [37]	2011	PES-PDA	81.6	94.5	76.7[c]	/
Chen [38]	2013	PES/HNTs-CS@Ag	375.6	97.6	/	94 (*E.coli*) 92.6 (*S.aureus*)[e]
Zhao [7]	2014	PES/F127-*b*-PDMS	~135	~100	>99.5	/
Zhao [6]	2013	PVDF/P(HFBM-SPP)	~92	~100	/	/
Kang [3]	2016	PVDF/MWNTs-g-CDDAC	94.7	93.6	97.8	92.7 (*E.coli*) 95.2 (*S.aureus*)

[a] Bovine serum albumin (BSA) rejection;
[b] Polyethylene glycol (M_w = 20,000 Da) rejection;
[c] Orange GII rejection;
[d] *E. coli*:*Escherichia coli*;
[e] *S. aureus*:*Staphylococcus aureus*.

against Gram-positive *Staphylococcus aureus* and Gram-negative *Escherichia coli*.

2. Materials and methods

2.1. Materials

Commercial grade PVDF powder (FR904) used as membrane material was obtained from Shanghai 3F New Material Co. Ltd. (China). 1-methyl-2-pyrrolidone (NMP) and polyvinyl pyrrolidone (PVP, M_w = 24,000 Da) were purchased from Shanghai Aladdin Chemical Agent Co. Ltd. (China). 5,5-dimethylhydantoin used as N-halamine epoxide precursor was obtained from Shanghai Hansi Chem. Ind. Co. Ltd. 3-chloropropyltriethoxysilane and sodium hypochlorite with 6–14% active chlorine content was purchased from Shanghai Aladdin Chemical Agent Co. Ltd. (China). Epichlorohydrin was obtained from Sigma-Aladdin (Shanghai) Trading Co. Ltd. MWNTs with a diameter of 20–40 nm and the average length of 5–15 μm were purchased from Shenzhen Nanotech Port Co. Ltd. (China). Sodium thiosulfate titration solution was purchased from Shanghai Lingfeng Chem. Co. Ltd. (China). Bovine serum albumin (BSA, M_w = 67,000 Da) was purchased from Shanghai Bio Co. Ltd. (China). Other chemicals were purchased from Shanghai Chemical Agent Company (China). Deionized (DI) water was used in all the experiments.

2.2. Purification and functionalization of MWNTs

Pristine MWNTs were purified using 0.5 M HCl aqueous solution for 1 h. After filtration, the mixtures were washed with pure water and dried at 40 °C. Next, the MWNTs were oxidized using HNO_3 at 160 °C for 6 h (denoted as O-MWNTs) [3]. The obtained O-MWNTs were sequentially washed with water and ethanol and dried at 40 °C.

2.3. Synthesis of 3-glycidyl-5, 5-dimethylhydantoin

Commercially available 5,5-dimethylhydantoin was used in this study. The derivative 3-glycidyl-5,5-dimethylhydantoin was synthesized in a two-step process (Scheme 1) [39]. Briefly, 0.05 mol 5, 5-dimethylhydantoin and 0.05 mol NaOH were dissolved in 40 mL of deionized water and agitated for 5–10 min at room temperature. Subsequently, 0.05 mol epichlorohydrin was added to the mixture and stirred for 10 h. Then, the majority of the water was removed from the mixture by rotation-evacuation, and the resultant hydantoin epoxide was dissolved in 50 mL of acetone and isolated by filtration to remove NaCl byproduct and acetone solvent. The crude 3-glycidyl-5, 5-dimethylhydantoin was obtained as an oil.

2.4. Preparation of N-Si-MWNTs

N-Halamine-containing MWNTs (N-MWNTs) were prepared from O-MWNTs as follows. First, the O-MWNTs were dispersed in 10% 3-glycidyl-5, 5-dimethylhydantoin solution with 1% NaOH for 30 min at 60 °C and sequentially cured at 60 °C for 1 h and 150 °C for 10 min. The subsequent procedure for N-MWNTs synthesis was similar to that illustrated in Scheme 1. The obtained N-MWNTs were soaked in 6 wt% 3-chloropropyltriethoxysilane aqueous solution for 15 min and cured for 1 h at 90 °C (Scheme 2) to achieve the final functionalized MWNTs (denoted as N-Si-MWNTs).

2.5. Preparation of PVDF hybrid membranes

The casting solutions were prepared with 16 wt% PVDF, 2 wt% PVP, and 0.3 wt% various functionalized MWNTs (O-MWNTs/N-MWNTs/N-Si-MWNTs) (Table 2), and the residual was balanced with NMP solvent. Homogeneous casting solutions were obtained by stirring for 12 h at 70 °C, followed by degassing for at least 6 h. The PVDF hybrid membranes were fabricated at 25 ± 1 °C via NIPS. A casting knife with a clearance of 200 μm was used to spread the casting solution, and the crude films were immediately immersed in coagulation liquid (deionized water) at 25 ± 1 °C. All the fabricated membranes were immersed in deionized water for 24 h to remove the residual solvent.

2.6. Characterization of PVDF hybrid membranes

2.6.1. Characterizations of functional MWNTs

Pristine MWNTs, O-MWNTs, and N-Si-MWNTs were examined using Fourier Transform Infrared Spectroscopy (FTIR, ElectronCorp Nicolet 380, San Jose, CA, USA) at 900–2000 cm^{-1}. The thermal stability of pristine MWNTs, O-MWNTs, and N-Si-MWNTs was evaluated by thermal gravimetric analysis (TGA, DSCQ100 TA Instruments, New Castle, DE, USA) at 35–800 °C with a heating rate of 10 °C/min.

2.6.2. Characterizations of PVDF hybrid membranes

The top surfaces, bottom surfaces, and cross-sections (broken in liquid nitrogen) of the PVDF hybrid membranes were detected by field emission scanning electron microscopy (FESEM, Hitachi S-4800, Tokyo, Japan). The surface roughness of the fabricated membranes was detected by atomic force microscopy (AFM, CSPM5500)

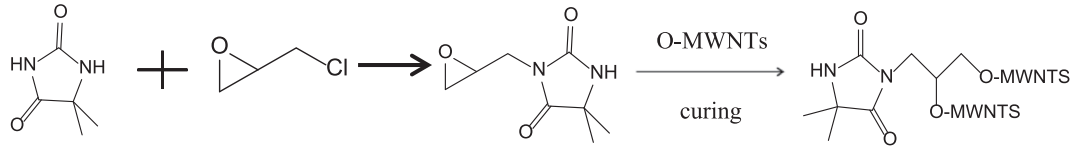

Scheme 1. Synthetic route of N-MWNTs.

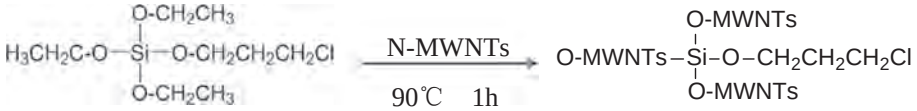

Scheme 2. Synthetic route of N-Si-MWNTs.

Table 2
Compositions of different casting solutions to fabricate the membranes (unit: wt%).

Membrane no.	PVDF	PVP	O-MWNTs	N-MWNTs	N-Si-MWNTs	NMP
M-0	16.0	2.0	/	/	/	82.0
M-1	16.0	2.0	0.3	/	/	81.7
M-2	16.0	2.0	/	0.3	/	81.7
M-3	16.0	2.0	/	/	0.3	81.7

under non-contact mode. In brief, the prepared membranes were cut into small squares, stuck on a glass substrate, and the roughness parameters of the membranes were quantified from the topography images with a scan size of 5 × 5 μm. The hydrophilicity of the PVDF hybrid membranes was measured by using sessile drop method on the outer surfaces with a contact angle analyzer (KRUSS DSA30, Hamburg, Germany). The contact angle experiments were conducted using a 3.0-μL droplet at ambient temperature. The initial contact angle was used to illustrate the surface hydrophilicity of the membranes. The membrane porosity ε (%) was calculated by using gravimetric method [40] as follows:

$$\varepsilon = \frac{\omega_1 - \omega_2}{a \times l \times d_w} \quad (1)$$

where ω_1 and ω_2 are the weights of wet and dry membrane samples, respectively, a is the membrane effective area (m^2), l is the membrane thickness (m), and d_w is the water density (0.998 g/cm^3).

The BSA rejections of the membranes were measured using an indigenous ultrafiltration system [24,41,42]. The fabricated membranes were pre-pressured with deionized water for 30 min at 2.0 bar to obtain a stable permeation flux before the analysis. After measuring the pure water permeability, the permeation and rejections for 500-ppm BSA aqueous solution were determined. The permeation flux for BSA aqueous solution was recorded as J_{BSA}. After ultrafiltration of the BSA aqueous solution, the fouled membranes were rinsed with deionized water for 30 min, and pure water permeability was again measured and recorded as J_R. The cyclic ultrafiltration and regeneration tests were used to evaluate the self-cleaning ability of the PVDF hybrid membranes. All the experiments were conducted at 1.0 bar and 25 ± 1 °C. The BSA concentrations in the feed and permeate flows were determined by ultraviolet and visible spectrophotometer (UV–Vis) at 280 nm. The rejections were calculated using Eq. (2). The pure water permeation flux (J_w) was defined as given in Eq. (3). The ability of recovery of the fouled membrane was determined based on the pure water FRR after BSA ultrafiltration, which was calculated using Eq. (4).

$$\mathrm{R}(\%) = 1 - \frac{C_p}{C_F} \times 100\% \quad (2)$$

$$J_w = \frac{Q}{a \times t} \quad (3)$$

$$\mathrm{FRR}(\%) = \frac{J_R}{J_w} \times 100\% \quad (4)$$

where R is the solute rejection, C_p and C_F are the concentrations of permeate and feed solutions, respectively, Q is the volumetric flow rate (m^3), a is the valid membrane area (m^2), J_R is the water flux of cleaned membrane after each cycle (m/s), and J_w is the initial pure water flux (m/s).

2.6.3. Resistance analysis

Darcy's Law was used to analyze mass transfer resistances during the ultrafiltration process, which can be expressed using Eq. (5) [43–45].

$$\mathrm{J} = \frac{\Delta P}{\mu R_t} = \frac{\Delta P}{\mu(R_m + R_{ir} + R_r)} \quad (5)$$

where J is the membrane permeation flux in the filtration process (m/s), ΔP is the transmembrane pressure (bar), μ is the filtrate viscosity (Pa S), R_t is the total permeation resistance of membrane (m^{-1}), R_m is the intrinsic membrane resistance, R_r is the reversible resistance (m^{-1}), and R_{ir} is the irreversible resistance (m^{-1}). Each resistance was calculated using Eqs. (6)–(9).

$$R_m = \frac{\Delta P}{\mu J_w} \quad (6)$$

$$R_t = \frac{\Delta P}{\mu J_{BSA}} \quad (7)$$

$$R_r = \frac{\Delta P}{\mu J_R} - R_m \quad (8)$$

$$R_{ir} = R_t - R_r - R_m \quad (9)$$

2.6.4. Oxidative chlorine content and antibacterial ability measurements

The standard iodometric/thiosulfate titration procedure was used to measure the immobilized oxidative chlorine on the mem-

brane samples [46]. The membrane samples were immersed in 0.5% NaClO solution and the pH was adjusted to 7 using HCl solution. After 45 min, the membrane samples were rinsed with deionized water and dried naturally at ambient temperature. Subsequently, about 1.0 g of the membrane sample was cut into pieces and immersed in 150 mL of sulfuric acid solution (0.04 mol/L) containing 0.5 g of potassium iodide and 0.4 mL of starch solution (0.5 wt%, acted as an indicator). Then, the mixture was titrated with sodium hyposulfite (0.01 mol/L) until the color transformed from blue to transparent. The positive chlorines (Cl^+) content of the membrane sample was calculated using Eq. (10):

$$Cl^+ = \frac{35.45 \times N \times V}{2 \times W} \times 100\% \quad (10)$$

where N is the normality (eq/L) of the consumed NaS_2O_3 in titration, V is the volume (L), and W is the weight of the sample.

The bacteriostatic efficiencies of the membranes were determined by using spread-plate method [47–49]. The optical density of the nutrient broth at 600 nm was measured to test the variation in the bacterial concentration after the sample was placed in a shake flask for 24 h. *E. coli* and *S. aureus* were respectively inoculated into Luria-Bertani (LB) growth medium and incubated overnight under agitation (250 rpm) at 37 °C. The optical densities of the two bacterial cultures at 600 nm (OD_{600}) were determined and adjusted to 0.6 using normal saline. Then, the *E. coli* and *S. aureus* cultures were diluted to 10^4 and 10^5 CFU/mL, respectively. For antibacterial assay, 1 mL of the bacterial culture was spread onto the sample membrane surface. After different periods of contact time, the membrane samples were cut into pieces and suspended in Eppendorf tubes containing 9 mL of normal saline. Then, 0.1 mL of the suspension was dispersed onto LB agar plates and incubated at 37 °C for 24 h. After incubation, the bacterial colonies on the plates were enumerated, and the sterilization ratio was calculated using Eq. (11):

$$E = \frac{(B - A)}{B} \times 100\% \quad (11)$$

where E is the sterilization ratio, A is the number of visible bacterial colonies with membrane contact, and B is the number of visible bacterial colonies without membrane contact.

3. Results and discussion

3.1. Characterizations of functionalized MWNTs

Fig. 1(a) shows the FTIR spectra of MWNTs, O-MWNTs, and N-Si-MWNTs. As shown in the figure, the shoulder at 1728 cm^{-1} and absorption peak at 1581 cm^{-1} for O-MWNTs corresponded to the vibrations of the —COOH groups, confirming that MWNTs were successfully oxidized [23]. The absorption peaks at 1718 cm^{-1} and 1766 cm^{-1} for N-Si-MWNTs corresponded to the carbonyl groups [50,51], and the bands at 1032 cm^{-1} could be attributed to Si—O, implying that the MWNTs were successfully functionalized with N-halamine and siloxane.

Fig. 1(b) illustrates the dispersion of MWNTs, O-MWNTs, and N-Si-MWNTs in deionized water for 7 days. Owing to high surface energy and nano size, the MWNTs tended to agglomerate and completely settle at the bottom of the flasks [52]. On the contrary, the O-MWNTs and N-Si-MWNTs were well dispersed in deionized water. This could be owing to the interactions between water and hydrophilic group as well as formation of a protective layer of carboxyl and hydroxyl groups preventing direct aggregation in the case of O-MWNTs [23], and existence of halamine group that enhances dispersion in water in the case of N-Si-MWNTs.

The TGA curves shown in Fig. 2 indicate the thermal stability of MWNTs, O-MWNTs, and N-Si-MWNTs. MWNTs exhibited the best

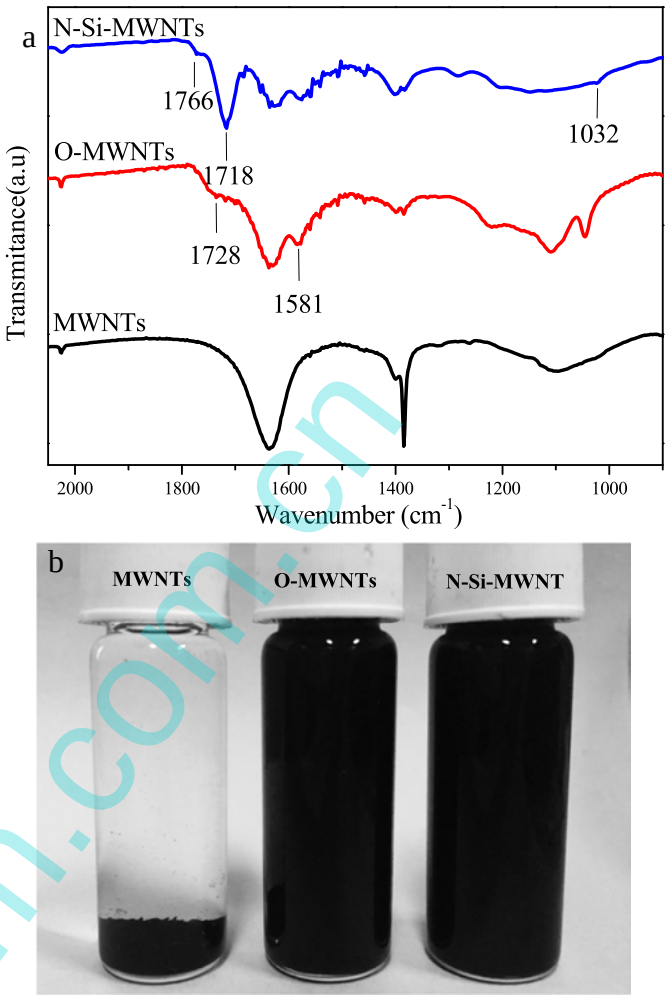

Fig. 1. The FTIR spectra of MWNTs, O-MWNTs and N-Si-MWNTs (a); the digital photos of MWNTs, O-MWNTs and N-Si-MWNTs suspend in deionized water standing for 7 days (b).

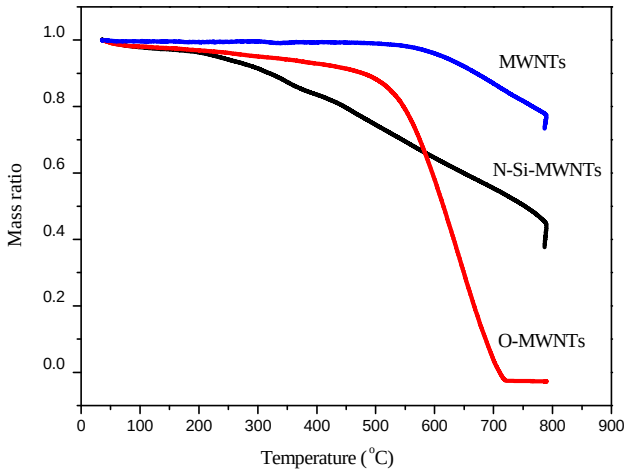

Fig. 2. The TGA curves of MWNTs, O-MWNTs and N-Si-MWNTs.

thermal stability and a decline in the TGA curve occurred at above 600 °C. With regard to O-MWNTs, the decline in the TGA curve could be divided into two sections. The first section below 250 °C could be attributed to the loss of adsorbed water and free water

in O-MWNTs, and the second section above 450 °C with a rapid decline could be attributed to the thermolysis of O-MWNTs. In the case of N-Si-MWNTs, the weight showed a downward trend from the beginning. The first section of the TGA curve below 250 °C corresponded to the loss of adsorbed water and free water in N-Si-MWNTs, and the second section of the curve could be ascribed to the thermolysis of hydantoin group. Furthermore, the decline in the TGA curve above 530 °C could be ascribed to the decomposition of carbon nanotubes. When compared with the TGA curves of MWNTs and O-MWNTs, that of N-Si-MWNTs presented an obvious decline trend, implying that the MWNTs surfaces were successfully grafted with functional groups [3].

3.2. Morphologies of PVDF hybrid membranes

The FESEM images of the top surfaces, bottom surfaces, and cross-sections of the PVDF hybrid membranes are presented in Fig. 3. No distinct variations in the top surfaces were observed, and the top surfaces of all the membranes appeared smooth and flat. Owing to strong non-solvent effect, the phase separation process immediately occurred on the top surfaces when the cast films were immersed in coagulation liquid (water). The bottom surfaces of the membranes were porous. As a result, the bottom surfaces adhered onto the glass, thus delaying the phase separation process when immersed in coagulation liquid. The demixing behavior resulted from the finger-like holes through the entire cross-section, which produced asymmetrical structure. The cross-sections of the membranes could be roughly segmented into three layers: skin layer, finger-like porous sub-layer, and macrovoid layer.

The top surfaces of the membranes were examined by AFM, as shown in Fig. 4. The antifouling ability of the membranes was associated with surface roughness, and the corresponding roughness parameters are presented in Table 3. The decrease in the R_a value from 9.79 nm (M-0) to 7.3 nm (M-1), 5.38 nm (M-2), and 4.49 nm (M-3) could be ascribed to the improved exchange of non-solvents and solvents during the phase inversion process owing to the addition of functionalized MWNTs [53]. It is generally accepted that membranes with flat surfaces possess higher antifouling ability [54]. The lower surface roughness could weaken the interaction between foulant and membranes. The R_q values of the membranes evidently decreased with the introduction of modified MWNTs. Surface skewness (R_{sk}) is the evaluation of symmetry of high distribution. For M-1 and M-2, the negative R_{sk} values corresponded to the dominance of valleys, whereas the positive skew values for M-0 and M-3 indicated that the peaks manage the surfaces. Surface kurtosis (R_{ku}) is a measure of the sharpness of height distribution. The R_{ku} values below 3 for M-3 indicated a repetitive and smooth surface, while those greater than 3 for M-0, M-1, and M-2 suggested a sharp height distribution [55].

3.3. The initial water contact angle and porosity of membranes

It is well known that surface hydrophilicity distinctly influences the permeability and antifouling ability of membranes. Fig. 5 shows the water contact angles of the top surfaces of the membranes. M-0 exhibited the largest water contact angle, demonstrating that raw PVDF membrane without the addition of modified MWNTs displayed the highest hydrophobicity. In comparison, the contact angles of membranes with modified MWNTs evidently decreased, establishing that the hydrophilicity of the hybrid membranes was increased. Both M-1 and M-2 presented similar water contact angles and best surface hydrophilicity among all the membranes owing to the addition of O-MWNTs and N-MWNTs, which resulted in interactions between the hydrophilic moieties (such as –COOH, $–R_2NH$) of the modified MWNTs and water molecules.

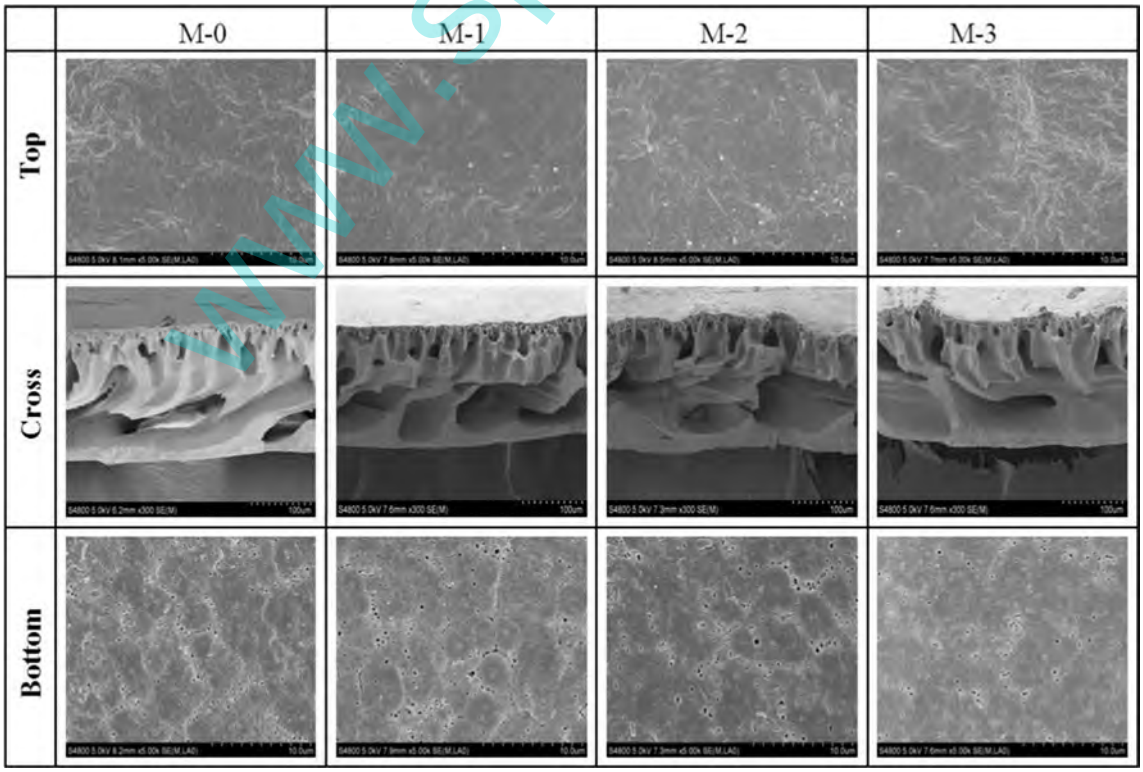

Fig. 3. The FESEM images top surfaces, cross sections and bottom surfaces of PVDF hybrid membranes.

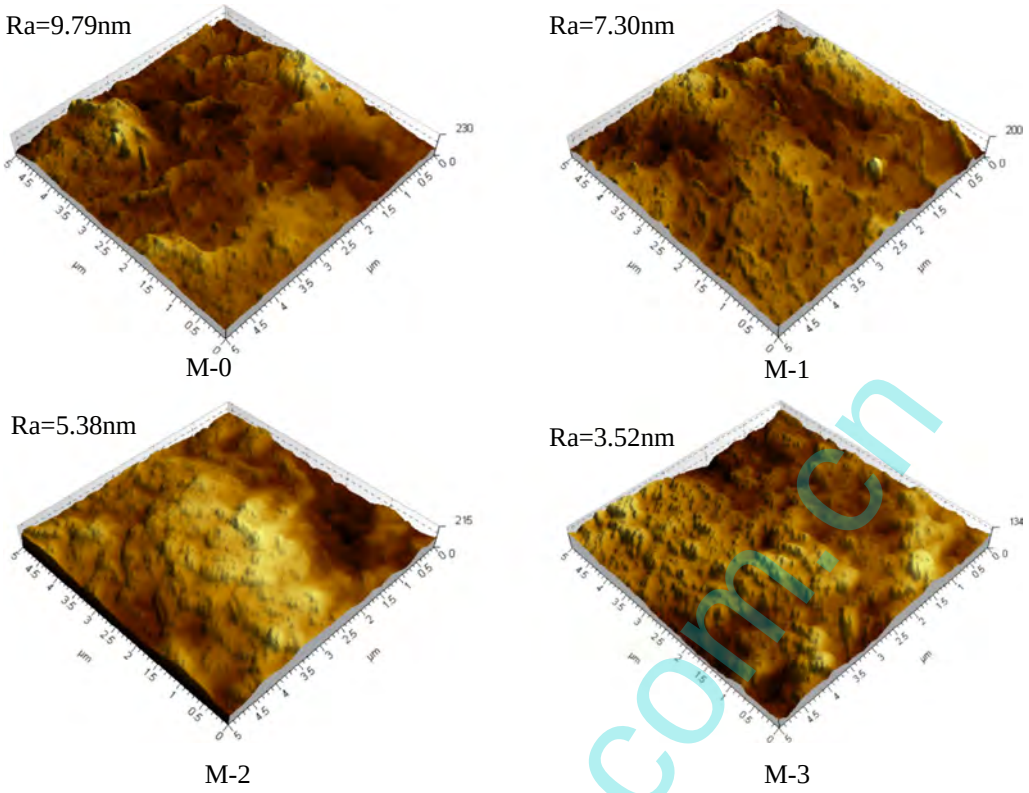

Fig. 4. Three-dimensional AFM images of tops surfaces of PVDF hybrid membranes.

Table 3
The roughness parameters of the top surfaces of PVDF hybrid membranes.

Membrane no.	R_a (nm)	R_q (nm)	R_{sk}	R_{ku}
M-0	9.79	13.00	0.653	3.69
M-1	7.30	9.55	-0.660	3.97
M-2	5.38	6.94	-0.842	3.99
M-3	3.52	4.29	0.030	2.54

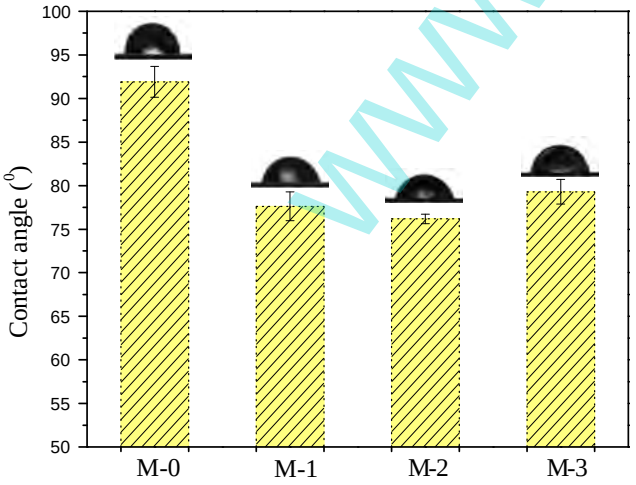

Fig. 5. The initial contact angles of PVDF hybrid membranes.

When compared with M-1 and M-2, the surface contact angle of M-3 was slightly increased owing to the introduction of silane groups with low surface energy in Si-N-MWNTs. The porosity of

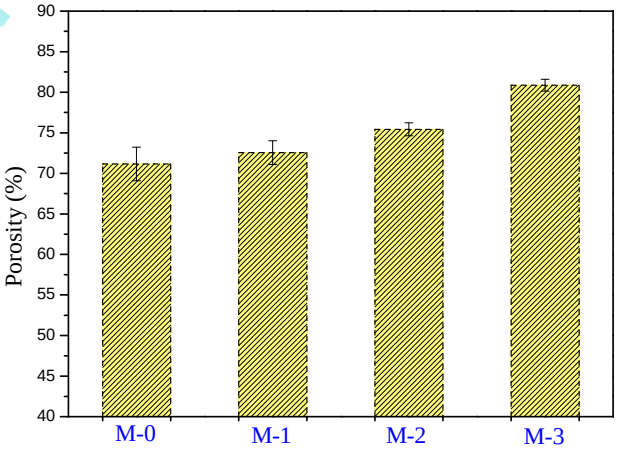

Fig. 6. The porosity of PVDF hybrid membranes.

the PVDF hybrid membranes is presented in Fig. 6. It can be seen from the figure that the porosity increased with the addition of modified MWNTs as a result of enhanced precipitation rate, which was conducive for the formation of porous membrane matrix and surfaces [41].

3.4. Permeation and self-cleaning properties of PVDF hybrid membranes

Fig. 7 shows the permeation fluxes of the PVDF hybrid membranes. The pure water permeation flux of raw PVDF membrane (M-0) was 126.3 $L{\cdot}M^{-2}{\cdot}h^{-1}{\cdot}bar^{-1}$. When compared with M-0, the other three membranes presented higher fluxes (161.8, 165.8,

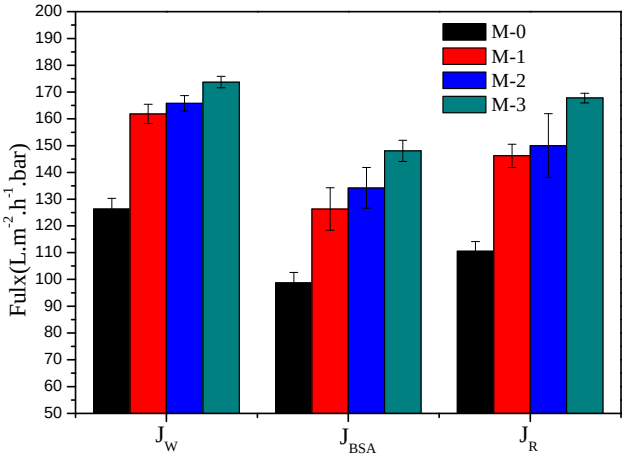

Fig. 7. The Permeation fluxes of membranes in the ultrafiltration of BSA solution.

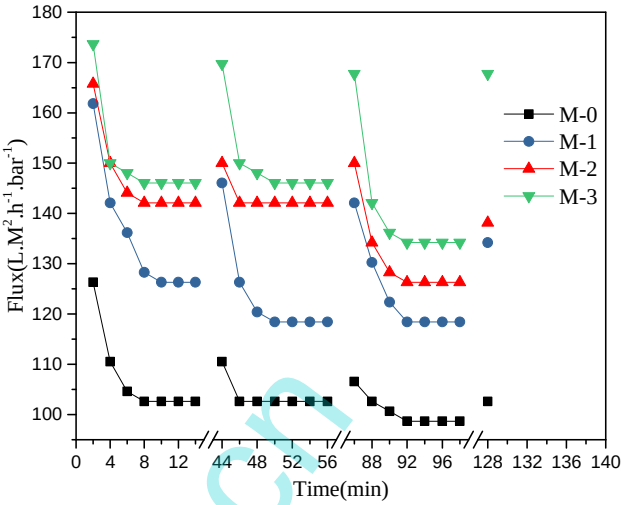

Fig. 8. Time-dependent flux of PVDF hybrid membranes with ultrafiltration-regeneration cycles.

and 173.7 $L{\cdot}M^{-2}{\cdot}h^{-1}{\cdot}bar^{-1}$ for M-1, M-2, and M-3, respectively) owing to the introduction of functionalized MWNTs in the membrane matrix. The lowest pure water permeation flux of M-0 could be attributed to the lowest surface hydrophilicity (Fig. 5) and lowest porosity (Fig. 6). Interestingly, the other membranes containing functionalized MWNTs presented similar pure water permeation fluxes varying from 161.8 to 173.7 $L{\cdot}M^{-2}{\cdot}h^{-1}{\cdot}bar^{-1}$. In general, the pure water permeation flux, BSA aqueous solution permeation flux, and recuperative pure water permeation flux presented an increase trend, which could be attributed to the addition of modified MWNTs.

The ultrafiltration–regeneration cycles of the PVDF hybrid membranes are illustrated in Fig. 8. After the ultrafiltration of BSA aqueous solution for a specific time period, the permeation fluxes of all the membranes sharply decreased owing to concentration polarization and membrane fouling. The FRRs of the membranes are listed in Table 4. When compared with the FRR value for M-3, those for M-0, M-1, and M-2 were much lower, especially in the third cycle. Besides, the FRR values for M-0, M-1, and M-2 gradually decreased in the three cycles, which were evidently different from those for M-3. M-3 exhibited the highest FRR value of above 96.5% after the entire ultrafiltration–regeneration cycles, which confirmed that the self-cleaning property of the PVDF/N-Si-MWNTs membranes (M-3) evidently improved with the addition of N-Si-MWNTs owing to decreased adhesion, resulting in easy removal of foulants. From Table 5, it can be noted that all the membranes examined possessed high BSA rejections, suggesting that the addition of MWNTs had no effect on BSA rejection.

The filtration resistances of the PVDF hybrid membranes were used to illustrate the underlying mechanism, and were calculated using Eqs. (6)–(9) (Fig. 9). As shown in Fig. 9, the presence of modified MWNTs in the PVDF hybrid membranes significantly reduced the permeation resistances. When compared with the permeation resistance of M-0, the observably reduced permeation resistances of M-3 could be ascribed to the addition of N-Si-MWNTs that enhanced the hydrophilicity and porosity of the membranes, ensuring water flux. Besides, siloxane prevented the adsorption of foulants, thus providing the membrane with self-cleaning ability.

A structural model was proposed (Fig. 10) to elucidate the antifouling and self-cleaning mechanism of PVDF/N-Si-MWNTs hybrid membranes. The PVDF/N-Si-MWNTs membrane surfaces presented optimal hydration energy and surface free energy, owing to the presence of hydrophilic groups (oxygen-containing functional groups and halamine groups), as well as low surface energy

Table 4
The flux recovery ratio of PVDF hybrid membranes.

Membrane no.	FRR/%		
	1st	2nd	3rd
M-0	87.4 ± 4.4	84.3 ± 5.3	81.2 ± 3.4
M-1	90.2 ± 3.9	87.8 ± 3.2	82.9 ± 4.5
M-2	90.4 ± 2.5	90.4 ± 4.7	83.3 ± 3.7
M-3	97.7 ± 3.1	96.5 ± 4.4	96.5 ± 4.0

brushes. As shown in Fig. 10, the protective hydration layer on the surface of the PVDF hybrid membranes effectively prevented direct interaction between foulants and membrane surfaces comprising hydrogen bonds. However, as indicated in Fig. 10(b), removal of some intractable adsorption of irresistible fouling on the membrane surface by rinsing with water was difficult, which was further ameliorated by convective flow-through membranes. Incorporation of low surface energy fouling-release moieties on membrane surfaces could offer the possibility of fabricating a superior antifouling surface. The final chemical structure could decrease the entropic and enthalpic driving forces for the adsorption of foulants and promote removal of the adsorbed foulants from the surfaces at moderate shear rate (Fig. 10(d)). These desired fouling-release properties could reduce both reversible and irreversible fouling and achieve high FRR with water rinsing [7].

3.5. Oxidative chlorine content and antibacterial measurement

The release of Cl^+ from N-halamine in N-MWNTs and N-Si-MWNTs contributed to the antibacterial ability of the membranes [56,57]. The Cl^+ contents in PVDF membranes are presented in Table 4. It can be observed from the table that the Cl^+ contents in M-2 and M-3 were 0.17 and 0.20 wt% with the addition of N-MWNTs and N-Si-MWNTs, respectively, which contributed to the bacteriostatic efficiency of the membranes.

The antibacterial efficacies of the PVDF hybrid membranes were determined using the spread-plate method. As shown in Fig. 11, the bacterial colonies of M-0 (Fig. 11(a) and (c)) occupied a large area of the Petri dish, suggesting that the raw PVDF membrane possessed no antibacterial effect against *S. aureus* and *E. coli*. In contrast, the hybrid membrane M-3 containing N-Si-MWNTs presented a dramatic decline in *S. aureus* and *E. coli* colonies, with

Table 5
The BSA rejection and the contents of Cl^+ of PVDF hybrid membranes.

Membrane no.	BSA rejections/%			Cl^+ wt.%
	1st	2nd	3rd	
M-0	95.5 ± 3.5	96.1 ± 1.1	97.8 ± 1.8	/
M-1	94.1 ± 2.1	96.2 ± 2.4	96.3 ± 1.3	/
M-2	94.5 ± 2.5	95.0 ± 1.0	96.7 ± 0.6	0.175 ± 0.017
M-3	95.7 ± 3.4	96.8 ± 0.2	97.1 ± 0.7	0.199 ± 0.030

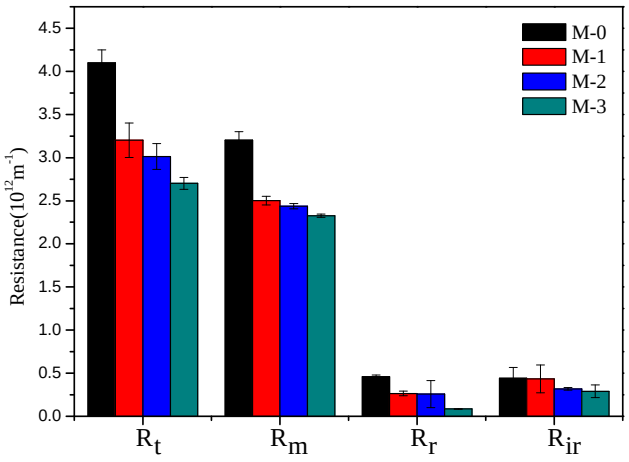

Fig. 9. Individual filtration resistance.

98.0% and 95.6% antibacterial efficacy, respectively, demonstrating the antibacterial properties of PVDF/N-Si-MWNTs membranes against both Gram-positive and Gram-negative bacteria. Based on the two antibacterial tests, it can be concluded that the PVDF/N-Si-MWNTs hybrid membranes presented excellent antibacterial efficiency against *S. aureus* and *E. coli*.

4. Conclusions

In the present study, novel versatile PVDF ultrafiltration membranes possessing both antibacterial and self-cleaning properties were fabricated. First, the MWNTs were modified with 3-glycidyl-5, 5-dimethylhydantoin and siloxane (N-Si-MWNTs), and then introduced onto the PVDF ultrafiltration membranes. The introduced modified MWNTs evidently enhanced the permeability, hydrophilicity, antibacterial property, and antifouling ability of the PVDF hybrid membranes. The hydraulic permeability of the membranes increased from 126.3 to 173.7 $L{\cdot}M^{-2}{\cdot}h^{-1}{\cdot}bar^{-1}$. During the BSA aqueous solution ultrafiltration–regeneration cycles, the PVDF/N-Si-MWNTs membranes showed an excellent FRR value above 96.5% even after three cycles, thus confirming the superior self-cleaning ability of these membranes. Furthermore, the fabricated PVDF/N-Si-MWNTs membranes presented outstanding antibacterial ability, with bacteriostatic efficacy reaching 98% and 95.6% against *S. aureus* and *E. coli*, respectively. The integrated properties including FRR values and bacteriostatic efficacy are evidently improved in comparison with the previous ultrafiltration membranes [34–38]. In conclusion, versatile PVDF ultrafiltration membranes with antibacterial, antifouling, and self-cleaning properties were successfully fabricated in this study, thus contributing to the field of membrane technology. The future study should be devoted to verifying the stability in antibacterial, antifouling and self-cleaning properties, and practical applications in water treatments.

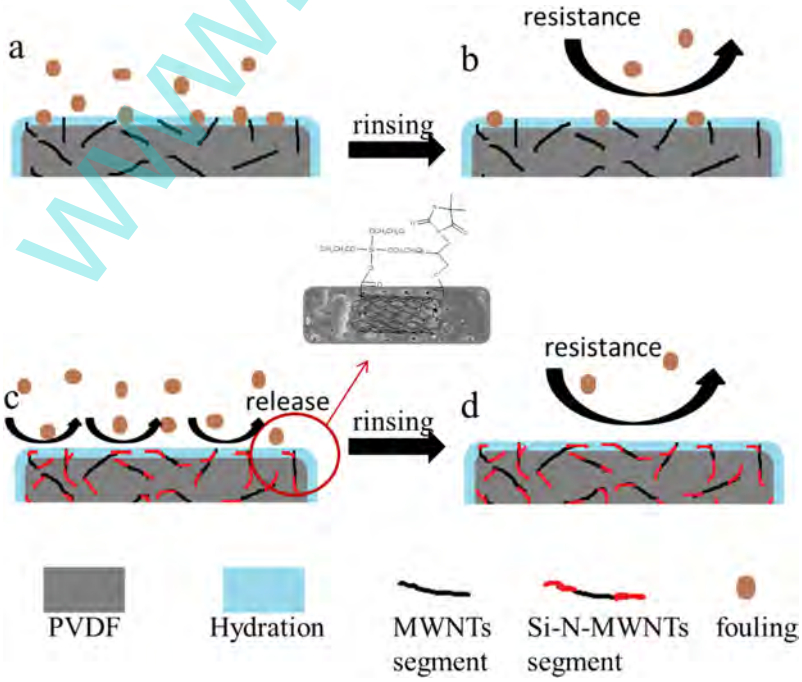

Fig. 10. Simple mechanism of the antifouling and self-cleaning properties (PVDF/MWNTs membranes (a, b); PVDF/N-Si-MWNTs membranes (c, d)).

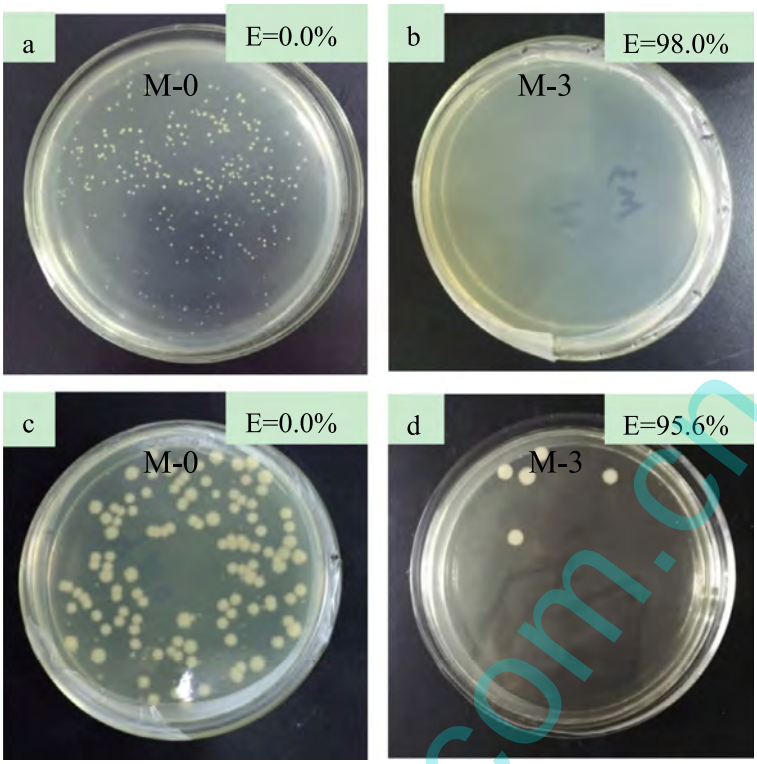

Fig. 11. The antibacterial efficiency against *S. aureus* (a, b) and *E. coli* (c, d) of PVDF/ N-Si-MWNTs membranes.

References

[1] J. Mansouri, S. Harrisson, V. Chen, Strategies for controlling biofouling in membrane filtration systems: challenges and opportunities, J. Mater. Chem. 20 (2010) 4567–4586.

[2] M. Lejars, A. Margaillan, C. Bressy, Fouling release coatings: a nontoxic alternative to biocidal antifouling coatings, Chem. Rev. 112 (2012) 4347–4390.

[3] B. Kang, Y.-D. Li, J. Liang, X. Yan, J. Chen, W.-Z. Lang, Novel PVDF hollow fiber ultrafiltration membranes with antibacterial and antifouling properties by embedding N-halamine functionalized multi-walled carbon nanotubes (MWNTs), RSC Adv. 6 (2016) 1710–1721.

[4] H.B. Kocer, S.D. Worley, R.M. Broughton, T.S. Huang, A novel N-halamine acrylamide monomer and its copolymers for antimicrobial coatings, React. Funct. Polym. 71 (2011) 561–568.

[5] X.-D. Weng, Y.-L. Ji, R. Ma, F.-Y. Zhao, Q.-F. An, C.-J. Gao, Superhydrophilic and antibacterial zwitterionic polyamide nanofiltration membranes for antibiotics separation, J. Membr. Sci. 510 (2016) 122–130.

[6] X. Zhao, W. Chen, Y. Su, W. Zhu, J. Peng, Z. Jiang, L. Kong, Y. Li, J. Liu, Hierarchically engineered membrane surfaces with superior antifouling and self-cleaning properties, J. Membr. Sci. 441 (2013) 93–101.

[7] X. Zhao, Y. Su, Y. Li, R. Zhang, J. Zhao, Z. Jiang, Engineering amphiphilic membrane surfaces based on PEO and PDMS segments for improved antifouling performances, J. Membr. Sci. 450 (2014) 111–123.

[8] R.A. Damodar, S.-J. You, H.-H. Chou, Study the self cleaning, antibacterial and photocatalytic properties of TiO_2 entrapped PVDF membranes, J. Hazard. Mater. 172 (2009) 1321–1328.

[9] C. Liao, P. Yu, J. Zhao, L. Wang, Y. Luo, Preparation and characterization of NaY/PVDF hybrid ultrafiltration membranes containing silver ions as antibacterial materials, Desalination 272 (2011) 59–65.

[10] H. Shi, F. Liu, L. Xue, Fabrication and characterization of antibacterial PVDF hollow fibre membrane by doping Ag-loaded zeolites, J. Membr. Sci. 437 (2013) 205–215.

[11] X. Li, R. Pang, J. Li, X. Sun, J. Shen, W. Han, L. Wang, In situ formation of Ag nanoparticles in PVDF ultrafiltration membrane to mitigate organic and bacterial fouling, Desalination 324 (2013) 48–56.

[12] A. Rahimpour, M. Jahanshahi, B. Rajaeian, M. Rahimnejad, TiO_2 entrapped nano-composite PVDF/SPES membranes: preparation, characterization, antifouling and antibacterial properties, Desalination 278 (2011) 343–353.

[13] I. Sawada, R. Fachrul, T. Ito, Y. Ohmukai, T. Maruyama, H. Matsuyama, Development of a hydrophilic polymer membrane containing silver nanoparticles with both organic antifouling and antibacterial properties, J. Membr. Sci. 387–388 (2012) 1–6.

[14] L. Yan, Y.S. Li, C.B. Xiang, Preparation of poly(vinylidene fluoride)(pvdf) ultrafiltration membrane modified by nano-sized alumina (Al_2O_3) and its antifouling research, Polymer 46 (2005) 7701–7706.

[15] L. Yan, Y.S. Li, C.B. Xiang, S. Xianda, Effect of nano-sized Al2O3-particle addition on PVDF ultratiltration membrane performance, J. Membr. Sci. 276 (2006) 162–167.

[16] H. Wu, J. Mansouri, V. Chen, Silica nanoparticles as carriers of antifouling ligands for PVDF ultrafiltration membranes, J. Membr. Sci. 433 (2013) 135–151.

[17] K. Goh, L. Setiawan, L. Wei, W. Jiang, R. Wang, Y. Chen, Fabrication of novel functionalized multi-walled carbon nanotube immobilized hollow fiber membranes for enhanced performance in forward osmosis process, J. Membr. Sci. 446 (2013) 244–254.

[18] P.-C. Ma, N.A. Siddiqui, G. Marom, J.-K. Kim, Dispersion and functionalization of carbon nanotubes for polymer-based nanocomposites: A review, Compos. A Appl. Sci. Manuf. 41 (2010) 1345–1367.

[19] M.J. Gallagher, H. Huang, K.J. Schwab, D.H. Fairbrother, B. Teychene, Generating backwashable carbon nanotube mats on the inner surface of polymeric hollow fiber membranes, J. Membr. Sci. 446 (2013) 59–67.

[20] B.P. Grady, Recent developments concerning the dispersion of carbon nanotubes in polymers, Macromol. Rapid Commun. 31 (2010) 247–257.

[21] V. Vatanpour, S.S. Madaeni, R. Moradian, S. Zinadini, B. Astinchap, Fabrication and characterization of novel antifouling nanofiltration membrane prepared from oxidized multiwalled carbon nanotube/polyethersulfone nanocomposite, J. Membr. Sci. 375 (2011) 284–294.

[22] E. Celik, H. Park, H. Choi, H. Choi, Carbon nanotube blended polyethersulfone membranes for fouling control in water treatment, Water Res. 45 (2011) 274–282.

[23] X. Zhang, W.-Z. Lang, H.-P. Xu, X. Yan, Y.-J. Guo, L.-F. Chu, Improved performances of PVDF/PFSA/O-MWNTs hollow fiber membranes and the synergism effects of two additives, J. Membr. Sci. 469 (2014) 458–470.

[24] N. Ghaemi, S.S. Madaeni, P. Daraei, H. Rajabi, T. Shojaeimehr, F. Rahimpour, B. Shirvani, PES mixed matrix nanofiltration membrane embedded with polymer wrapped MWCNT: Fabrication and performance optimization in dye removal by RSM, J. Hazard. Mater. 298 (2015) 111–121.

[25] Z.-Z. Kang, B. Zhang, Y.-C. Jiao, Y.-H. Xu, Q.-Z. He, J. Liang, High-efficacy antimicrobial cellulose grafted by a novel quaternarized N-halamine, Cellulose 20 (2012) 885–893.

[26] K. Tan, S.K. Obendorf, Fabrication and evaluation of electrospun nanofibrous antimicrobial nylon 6 membranes, J. Membr. Sci. 305 (2007) 287–298.

[27] K. Tan, S.K. Obendorf, Development of an antimicrobial microporous polyurethane membrane, J. Membr. Sci. 289 (2007) 199–209.

[28] X. Wei, Z. Wang, J. Chen, J. Wang, S. Wang, A novel method of surface modification on thin-film-composite reverse osmosis membrane by grafting hydantoin derivative, J. Membr. Sci. 346 (2010) 152–162.

[29] S. Sommer, A. Ekin, D.C. Webster, S.J. Stafslien, J. Daniels, L.J. VanderWal, S.E. Thompson, M.E. Callow, J.A. Callow, A preliminary study on the properties and fouling-release performance of siloxane-polyurethane coatings prepared from poly(dimethylsiloxane) (PDMS) macromers, Biofouling 26 (2010) 961–972.

[30] S. Krishnan, N. Wang, C.K. Ober, J.A. Finlay, M.E. Callow, J.A. Callow, A. Hexemer, K.E. Sohn, E.J. Kramer, D.A. Fischer, Comparison of the fouling release properties of hydrophobic fluorinated and hydrophilic PEGylated block copolymer surfaces: attachment strength of the diatom Navicula and the green alga Ulva, Biomacromolecules 7 (2006) 1449–1462.
[31] J.C. Yarbrough, J.P. Rolland, J.M. DeSimone, M.E. Callow, J.A. Finlay, J.A. Callow, Contact angle analysis, surface dynamics, and biofouling characteristics of cross-linkable, random perfluoropolyether-based graft terpolymers, Macromolecules 39 (2006) 2521–2528.
[32] S. Krishnan, C.J. Weinman, C.K. Ober, Advances in polymers for anti-biofouling surfaces, J. Mater. Chem. 18 (2008) 3405.
[33] R.F. Brady, I.L. Singer, Mechanical factors favoring release from fouling release coatings, Biofouling 15 (2000) 73–81.
[34] J. Liu, X. Shen, Y. Zhao, L. Chen, Acryloylmorpholine-grafted PVDF membrane with improved protein fouling resistance, Ind. Eng. Chem. Res. 52 (2013) 18392–18400.
[35] L. Duan Q. Zhao J. Liu Y. Zhang Antibacterial behavior of halloysite nanotubes decorated with copper nanoparticles in a novel mixed matrix membrane for water purification, Environ. Sci.: Water Res. Technol., 1 (2015) 874-881.
[36] X. Li, T. Cai, T.-S. Chung, Anti-fouling behavior of hyperbranched polyglycerol-grafted poly(ether sulfone) hollow fiber membranes for osmotic power generation, Environ. Sci. Technol. 48 (2014) 9898–9907.
[37] Y. Li, Y. Su, X. Zhao, X. He, R. Zhang, J. Zhao, X. Fan, Z. Jiang, Antifouling High-Flux Nanofiltration Membranes Enabled by Dual Functional Polydopamine, ACS Appl. Mater. Interfaces 6 (2011) 5548–5557.
[38] Y. Chen, Y. Zhang, H. Zhang, J. Liu, C. Song, Biofouling control of halloysite nanotubes-decorated polyethersulfone ultrafiltration membrane modified with chitosan-silver nanoparticles, Chem. Eng. J. 228 (2013) 12–20.
[39] J. Liang, Y. Chen, X. Ren, R. Wu, K. Barnes, S.D. Worley, R.M. Broughton, U. Cho, H. Kocer, T.S. Huang, Fabric treated with antimicrobial N-halamine epoxides, Ind. Eng. Chem. Res. 46 (2007) 6425–6429.
[40] M. Safarpour, A. Khataee, V. Vatanpour, Effect of reduced graphene oxide/TiO_2 nanocomposite with different molar ratios on the performance of PVDF ultrafiltration membranes, Sep. Purif. Technol. 140 (2015) 32–42.
[41] W.-Z. Lang, Q. Ji, J.-P. Shen, Y.-J. Guo, Z.-L. Xu, The roles of alkali metal counter-ions of PFSA play in the formation of PVDF/PFSA-M hollow fiber membranes, Desalination 292 (2012) 45–52.
[42] W.-Z. Lang, Z.-L. Xu, H. Yang, W. Tong, Preparation and characterization of PVDF–PFSA blend hollow fiber UF membrane, J. Membr. Sci. 288 (2007) 123–131.
[43] S. Liang, L. Qu, F. Meng, X. Han, J. Zhang, Effect of sludge properties on the filtration characteristics of self-forming dynamic membranes (SFDMs) in aerobic bioreactors: Formation time, filtration resistance, and fouling propensity, J. Membr. Sci. 436 (2013) 186–194.
[44] J. Nimhurchu, G. Foley, Dead-end filtration of yeast suspensions: Correlating specific resistance and flux data using artificial neural networks, J. Membr. Sci. 281 (2006) 325–333.
[45] J. Wang, W.-Z. Lang, H.-P. Xu, X. Zhang, Y.-J. Guo, Improved poly(vinyl butyral) hollow fiber membranes by embedding multi-walled carbon nanotube for the ultrafiltrations of bovine serum albumin and humic acid, Chem. Eng. J. 260 (2015) 90–98.
[46] B. Zhang, Y. Jiao, Z. Kang, K. Ma, X. Ren, J. Liang, Durable antimicrobial cotton fabrics containing stable quaternarized N-halamine groups, Cellulose 20 (2013) 3067–3077.
[47] L. Duan, W. Huang, Y. Zhang, High-flux, antibacterial ultrafiltration membranes by facile blending with N-halamine grafted halloysite nanotubes, Rsc Advances 5 (2015) 6666–6674.
[48] L. Huang, S. Zhao, Z. Wang, J. Wu, J. Wang, S. Wang, In situ immobilization of silver nanoparticles for improving permeability, antifouling and anti-bacterial properties of ultrafiltration membrane, J. Membr. Sci. 499 (2016) 269–281.
[49] Q. Cai, S. Bao, Y. Zhao, T. Zhao, L. Xiao, G. Gao, H. Chokto, A. Dong, Tailored synthesis of amine N-halamine copolymerized polystyrene with capability of killing bacteria, J. Colloid Interface Sci. 444 (2015) 1–9.
[50] X. Cheng, K. Ma, R. Li, X. Ren, T.S. Huang, Antimicrobial coating of modified chitosan onto cotton fabrics, Appl. Surf. Sci. 309 (2014) 138–143.
[51] I. Cerkez, H.B. Kocer, S.D. Worley, R.M. Broughton, T.S. Huang, N-halamine copolymers for biocidal coatings, React. Funct. Polym. 72 (2012) 673–679.
[52] V. Datsyuk, M. Kalyva, K. Papagelis, J. Parthenios, D. Tasis, A. Siokou, I. Kallitsis, C. Galiotis, Chemical oxidation of multiwalled carbon nanotubes, Carbon 46 (2008) 833–840.
[53] I.M. Wienk, R.M. Boom, M.A.M. Beerlage, A.M.W. Bulte, C.A. Smolders, H. Strathmann, Recent advances in the formation of phase inversion membranes made from amorphous or semi-crystalline polymers, J. Membr. Sci. 113 (1996) 361–371.
[54] L.-Y. Yu, Z.-L. Xu, H.-M. Shen, H. Yang, Preparation and characterization of PVDF–SiO_2 composite hollow fiber UF membrane by sol–gel method, J. Membr. Sci. 337 (2009) 257–265.
[55] J. Stawikowska, A.G. Livingston, Assessment of atomic force microscopy for characterisation of nanofiltration membranes, J. Membr. Sci. 425–426 (2013) 58–70.
[56] A. Dong, S. Lan, J. Huang, T. Wang, T. Zhao, W. Wang, L. Xiao, X. Zheng, F. Liu, G. Gao, Y. Chen, Preparation of magnetically separable N-halamine nanocomposites for the improved antibacterial application, J. Colloid Interface Sci. 364 (2011) 333–340.
[57] H. Yu, X. Zhang, Y. Zhang, J. Liu, H. Zhang, Development of a hydrophilic PES ultrafiltration membrane containing SiO_2@N-Halamine nanoparticles with both organic antifouling and antibacterial properties, Desalination 326 (2013) 69–76.